Contactin-1 regulates myelination and nodal/paranodal domain organization in the central nervous system

Gülsen Çolakoğlu[a,1], Ulrika Bergstrom-Tyrberg[a,b,1], Erik O. Berglund[a,2], and Barbara Ranscht[a,3]

[a]Sanford-Burnham Medical Research Institute, La Jolla, CA 92037; and [b]Neurogenetics Unit, Department of Molecular Medicine and Surgery, Center for Molecular Medicine, Karolinska Institutet, S-17176 Stockholm, Sweden

Edited by Ben A. Barres, Stanford University, Stanford, CA, and approved November 4, 2013 (received for review July 22, 2013)

Myelin, a multilayered membrane sheath formed by oligodendrocytes around axons in the CNS, enables rapid nerve impulse conduction and sustains neuronal health. The signals exchanged between axons and oligodendrocytes in myelin remain to be fully elucidated. Here we provide genetic evidence for multiple and critical functions of Contactin-1 in central myelin. We document dynamic Contactin-1 expression on oligodendrocytes in vivo, and progressive accumulation at nodes of Ranvier and paranodes during postnatal mouse development. Nodal and paranodal expression stabilized in mature myelin, but overall membranous expression diminished. Contactin-1–deficiency disrupted paranodal junction formation as evidenced by loss of Caspr, mislocalized potassium $K_v1.2$ channels, and abnormal myelin terminal loops. Reduced numbers and impaired maturation of sodium channel clusters accompanied this phenotype. Histological, electron microscopic, and biochemical analyses uncovered significant hypomyelination in Contactin-1–deficient central nerves, with up to 60% myelin loss. Oligodendrocytes were present in normal numbers, albeit a minor population of neuronal/glial antigen 2-positive ($NG2^+$) progenitors lagged in maturation by postnatal day 18, when the mouse null mutation was lethal. Major contributing factors to hypomyelination were defects in the generation and organization of myelin membranes, as judged by electron microscopy and quantitative analysis of oligodendrocyte processes labeled by GFP transgenically expressed from the proteolipid protein promoter. These data reveal that Contactin-1 regulates both myelin formation and organization of nodal and paranodal domains in the CNS. These multiple roles distinguish central Contactin-1 functions from its specific role at paranodes in the periphery, and emphasize mechanistic differences in central and peripheral myelination.

The rapid integration of sensory, motor, and cognitive functions within the nervous system of higher vertebrates depends on the ability of neurons to propagate nerve impulses with high velocity. This process is accomplished by electrical insulation of axons with myelin, a multilamellar membrane sheath formed by oligodendrocytes in the CNS. Oligodendrocytes each enwrap multiple axons with myelin, and convey signals that regulate axon diameter and neuronal health (1, 2). Reverse communication from axons affects oligodendrocyte numbers, maturation, and survival (3, 4). Loss of central myelin is a major cause for neuronal dysfunctions and degeneration in demyelinating diseases, including multiple sclerosis (5). Effective regenerative treatments that compensate for myelin damage and preserve neuronal functions in multiple sclerosis remain to be established. Deciphering the molecular signals exchanged between axons and oligodendrocytes in developing myelin is an essential step toward understanding the mechanisms that will guide future repair strategies (6, 7).

Contactin-1 (hereafter referred to as Contactin), a glycosylphosphatidyl inositol (GPI)-linked membrane glycoprotein, is a prime candidate to mediate neuron–glia communication in central myelin. Contactin is expressed by a diversity of neurons and contributes to the formation and function of neuronal connections (8–10). In myelinated peripheral nerves, Contactin is concentrated at axon membranes flanking the nodes of Ranvier, and serves an essential role in organizing the septate-like paranodal axoglial junctions (11, 12). Formation of these junctions is crucial for domain organization of myelinated nerves to enable rapid propagation of nerve impulses. Contactin supports junction formation by associating the paranodal transmembrane protein Caspr and transporting the complex to the axolemma where interactions with glial neufoascin-155 regulate clustering and junction formation (12–15). In central myelin, Contactin delineates both nodes of Ranvier and paranodes (11, 16). Cultured oligodendrocytes also express Contactin, which up-regulates myelin-basic protein (MBP) mRNA translation and differentiation when stimulated with recombinant L1-ligand protein (17–19). The functions of Contactin in central myelination, and in particular possible contributions of Contactin expressed by oligodendrocytes, have not been reported.

Here we validate the expression of Contactin by oligodendrocytes in vivo, and investigate Contactin's contribution to central myelin formation in null mutant mice (*Cntn1*-KO). We report dynamic Contactin expression on axons and oligodendrocytes during postnatal mouse development. Our data provide genetic evidence for Contactin in oligodendrocyte membrane extension and myelination, nodal formation and maturation, and paranodal domain establishment. These multiple, interrelated roles of Contactin in central myelin extend beyond Contactin's reported function in paranodal junction formation in the peripheral nervous system (PNS) (12), and highlight its key role in the communication between axons and oligodendrocytes that enable efficient formation of functional myelin in the CNS.

Significance

Myelin is a multilayered membrane sheath that encircles axons to enable rapid information processing and protect neurons. Formation of myelin requires communication between axons and oligodendrocytes, the myelin-forming cells in the CNS. Here we identify Contactin-1 as a critical signal for axon–glia communication in CNS myelin. Gene ablation in mice shows that Contactin-1 is necessary for myelin sheath formation by oligodendrocytes and establishment of paranodal axoglial junctions that regulate the domain organization and enable rapid nerve impulse conduction of myelinated nerves. The multiple and critical aspects of Contactin-1 in central myelin formation identified in the current study will guide novel approaches aimed at enhancing regeneration in demyelinating diseases that specifically affect the CNS.

Author contributions: G.Ç., E.O.B., and B.R. designed research; G.Ç., U.B.-T., and E.O.B. performed research; G.Ç., U.B.-T., and B.R. analyzed data; and G.Ç. and B.R. wrote the paper.

The authors declare no conflict of interest.

This article is a PNAS Direct Submission.

[1]G.Ç. and U.B.-T. contributed equally to the experiments.

[2]Present address: Gilead Sciences, Inc., Foster City, CA 94404.

[3]To whom correspondence should be addressed. E-mail: ranscht@sanfordburnham.org.

Results

Contactin Is Distributed at Nodes, Paranodes, and Glial Membranes in Central Myelin. Earlier studies of central myelinated nerves described Contactin's distribution at nodes of Ranvier and paranodes (11, 16). Contactin is also strongly expressed by developing oligodendrocytes in culture (17–19), but its distribution on oligodendrocytes in myelinated nerves has remained obscure. We therefore asked whether oligodendrocytes in vivo express Contactin. We varied the fixation and immunohistochemical staining conditions for Contactin detection in optic nerves at two time points: during active myelinogenesis at postnatal day (P)18 and in mature myelin at P28. Results are summarized in Table 1. Staining at nodes and paranodes as highlighted in the literature was detected at P28 by fixing tissues with 4% (wt/vol) paraformaldehyde (PFA) and subsequent extraction with 100% (vol/vol) methanol (Fig. 1) (+MOH 5-h fix). When methanol was omitted, more extensive Contactin staining that varied depending on animal age and duration of fixation was detected. Specifically, at P18 fixation with 4% PFA preserved strong Contactin staining on loose membranes (Fig. 1) (–MOH 3-h/5-h fix). Increasing stringency (100% methanol treatment after 4% PFA fixation; +MOH 5-h fixation) extracted most of the Contactin signal from membranous structures but sustained signals at nodal and paranodal domains. At P28, the membranous signal was weaker after 1–5 h of PFA fixation, suggesting that Contactin is either down-regulated or redistributed during oligodendrocyte membrane expansion. Nodal Contactin was visualized after 3 h or more of PFA fixation and was unaffected by methanol extraction. At both P18 and P28, the nodal signal was more pronounced with longer PFA fixation times (Fig. 1 and Table 1) (−MOH 5-h fix). Paranodal Contactin was apparent in developing optic nerves at P18 even after 1-h PFA fixation (Table 1). However, access to the tightened paranodal axoglial complex at P28 required further extraction, achieved here with methanol. With methanol extraction, Contactin was prominent only at nodes and paranodes. Both the nodal and paranodal Contactin signals condensed into tight clusters with the developmental stabilization of these domains. Staining under all reported conditions was specific and not observed in *Cntn1*-KO mice and in controls lacking primary antibodies. These data illustrate that detection of Contactin depends on the staining conditions and support expression beyond nodes and paranodes in myelin.

Table 1. Contactin staining optimization using WT mouse optic nerves

	Without methanol		With methanol*	
Fixation time† →	1 h	5 h	1 h	5 h
P18				
Paranodes	+ +	+		+ +
Nodes	—	+ +		+ +
Elsewhere	+ +	+ + +		+
P28/30				
Paranodes	+	—	+ + +	+ +
Nodes	—	+ + +	—	+ +
Elsewhere	+	+ +	+	+

Contactin staining was optimized using optic nerves from WT P18 and P28–30 mice. Four different protocols were carried out: 1-h fixation with 4% PFA, 5-h fixation with 4% PFA, 1-h fixation with 4% PFA followed by 10-min methanol extraction, and 5-h fixation with 4% PFA followed by 10-min methanol extraction. Staining results are reported as +++ (very good), ++ (good), + (weak), or — (none), which are all relative to each other.
*Extraction using 100% ice-cold methanol for 10 min.
†Fixation using 4% PFA.

Contactin Delineates Oligodendrocyte Progenitor Cells and Is Down-Regulated from Mature Myelin. To test if the observed membranous Contactin staining in myelinated optic nerves relates to cells of the oligodendrocyte lineage, we performed triple immunostaining for Contactin with neuronal/glial antigen-2 (NG2) and adenomatous polyposis coli (APC), markers for oligodendrocyte progenitor cells (OPC) and mature oliogodendrocytes, respectively. Optic nerve tissue harvested between P10 and P30 was immersion-fixed for 3 h in 4% PFA without methanol extraction to preserve Contactin on membranous structures. At P10, Contactin clearly delineated $NG2^+$ migrating and differentiating oligodendrocytes, whereas APC^+ oligodendrocyte somata did not present discernable Contactin staining (Fig. 2). In Fig. 2*B*, a single oligodendrocyte outlined by NG2 expression shows overlapping staining for Contactin on the cell body and on proximal but not distal processes. At P10, Contactin was undetectable on optic axons that by this time point had innervated their targets (20, 21). At P16, a dramatic change in pattern occurred, with prominent Contactin staining now delineating parallel running structures resembling myelin membranes. At this developmental stage, Contactin staining also began to discriminate developing paranodes (Fig. 2*A*). By P18, the progressively refined Contactin pattern clearly distinguished the nodes and the tightly clustered, double-barrel structures typical for paranodes bilaterally flanking the nodes of Ranvier, whereas staining on loose membranous structures diminished. Contactin was also observed at nodes of Ranvier at this time point (Fig. 1). By P28–30, overall Contactin staining declined even more but prominent expression was detected at nodes after 3-h fixation in 4% PFA, as shown in Fig. 2*A*, and at paranodes after PFA plus methanol treatment, as shown in Fig. 1 (see also Table 1). These dynamic developmental changes indicate that Contactin, in addition to its expression at nodes and paranodes, delineates migrating, premyelinating, and myelinating oligodendrocytes, and is down-regulated from mature myelin.

Hypomyelination in the CNS of *Cntn1*-KO Mice. To assess the contribution of Contactin in central myelin formation, we analyzed *Cntn1*-KO mice between the onset of myelination at P10 up to P18, when the mutation is lethal (10). Absence of Contactin in *Cntn1*-KO mice was confirmed by immunostaining of optic nerve, cerebellum, and corpus callosum, and by Western blotting of whole-brain lysates (Fig. 3 *A* and *B*).

To determine the extent of myelin formed in the absence of Contactin, we examined different brain regions of P18 WT and *Cntn1*-KO mice. Gallyas silver staining revealed significant myelin reduction in optic nerves (27% reduction, WT $n = 6$, KO $n = 3$, $P < 0.05$) and corpus callosum (38% reduction, WT $n = 6$, KO $n = 3$, $P < 0.05$) of *Cntn1*-KO mice compared with WT (Fig. 3*C*). Consistently, Western blotting analysis of whole-brain lysates from *Cntn1*-KO and WT mice showed 50% reduced MBP expression in the mutant condition (Fig. 3*B*) ($n = 3$, $P < 0.05$). Staining for MBP confirmed the reduction of myelin in corpus callosum of KO compared with WT mice (Fig. 3*C*). Thus, the hypomyelination phenotype was apparent in multiple areas of *Cntn1*-KO CNS.

Contactin Affects Myelin Development in Optic Nerves. To examine the cellular defects underlying myelin loss in *Cntn1*-KO mice, we turned to developing optic nerves. Cross-sections of matching regions of P11 and P18 *Cntn1*-KO and WT nerves revealed overall decreased nerve diameters in the mutant condition (Fig. 4 *A* and *B*). Neurofilament-200 (NF200), a marker for mature axons (22, 23), was expressed at reduced levels in *Cntn1*-KO nerves, consistent with the suggestion that the mutation affected axon maturation (Fig. 4 *A* and *C*).

Examinations at the ultrastructural level provided more detailed insights. Cross-sectioned P16 optic nerves showed an overt

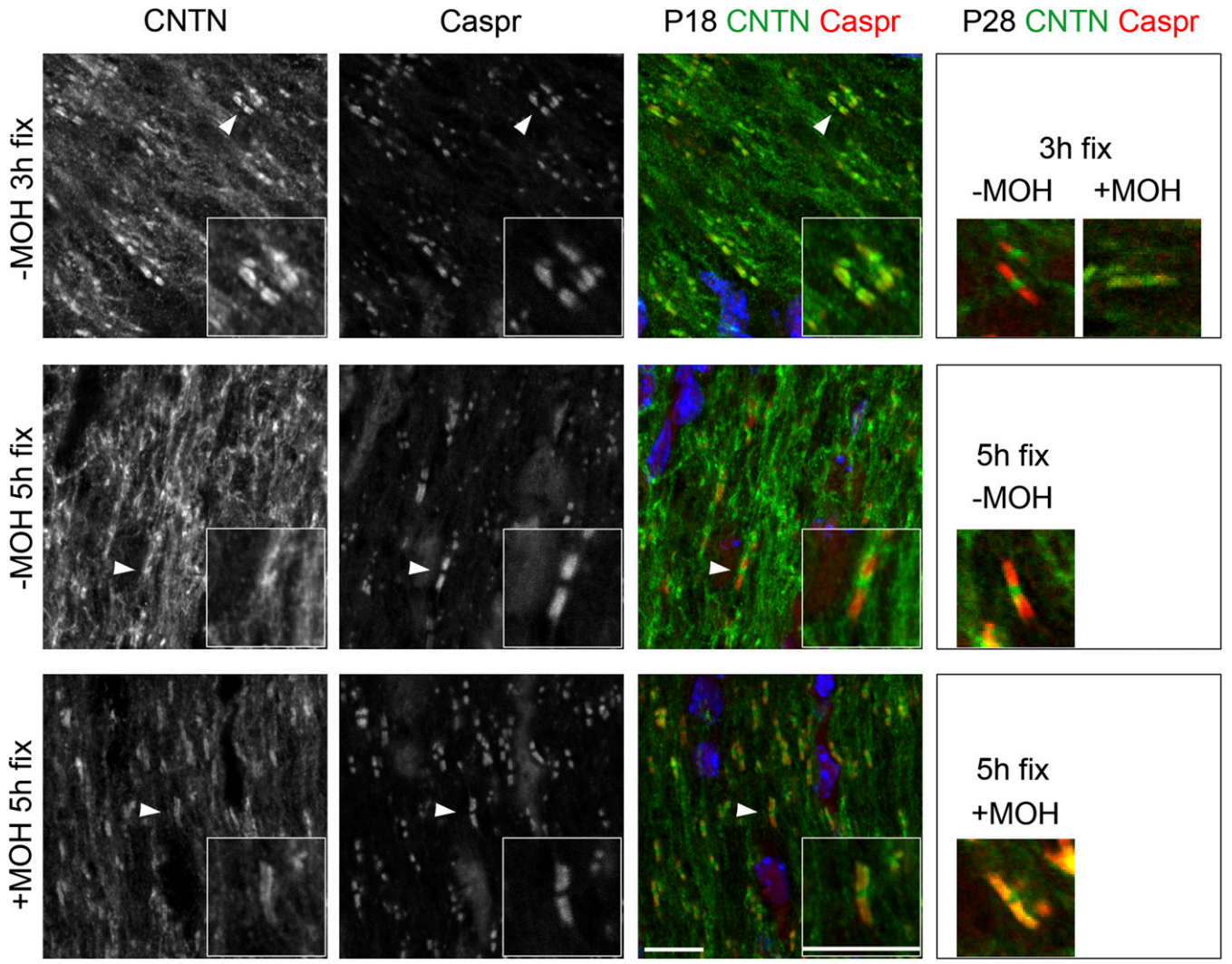

Fig. 1. Contactin expression at nodes, paranodes, and glial membranes in central myelin. Contactin staining was optimized using WT P18 and P28 mice. Optic nerves were fixed for 3 or 5 h with 4% PFA, and used untreated (−MOH) or after treatment with methanol (+MOH). Paranodes were identified with recombinant human anti-Caspr antibodies. Subimages are details of P18 paranodes pointed out with white arrowheads. Under low stringency conditions (−MOH), Contactin localized at the nodes, paranodes, and on noncompacted membranes. Increased fixation time preserved predominantly nodal Contactin staining. Methanol extraction improved paranodal staining, but extensively reduced Contactin signal elsewhere (see Table 1 for more details). (Scale bars, 10 μm.)

decrease in the number of myelinated fibers in *Cntn1*-KO mice (Fig. 4*D*). In the WT, 54% of all axons were myelinated at P16, whereas only 21% of the axons were wrapped with myelin in the KO condition (counted total >1,200 axons for WT and >2,400 axons for KO). This result reflects almost 60% reduction in the number of axons enwrapped by myelin in Contactin-deficient optic nerves. To better understand this defect, we quantified the percentage of myelinated axons according to their diameter using nonoverlapping regions from electron micrographs. In the KO condition, we observed that reduced myelination predominantly affected the smaller-diameter axons (<0.6 μm) (Fig. 4*E*) ($P < 0.05$). The proportion of unmyelinated small-diameter axons was increased in the mutant mice (120 vs. 70 axons per area unit for KO and WT, respectively) consistent with decreased NF200 staining. Quantifying the percentage of axons with respect to diameter, we noted an increased ratio of smaller-diameter axons (0.2–0.4 μm) and reduced ratios for larger-diameter axons for KO nerves (Fig. 4*F*). Thus, *Cntn1*-KO developing optic nerves harbored more immature small-diameter and fewer large-diameter axons than their WT counterparts, and showed decreased total myelination that particularly affected the small-diameter axons. These data are consistent with the suggestion that Contactin-mediated interactions contribute to the regulation of axon diameter and myelination.

OPC Maturation and Impaired Myelin Membrane Expansion in *Cntn1*-KO Optic Nerves. To gain insights into the cellular dysfunctions causing myelin loss in *Cntn1*-KO mice, we asked whether sufficient numbers of oligodendrocytes are in position to myelinate optic axons. Immunohistochemical analyses combined with DAPI staining determined the percentage of mature oligodendrocytes expressing the APC marker during postnatal nerve development. The number of APC^+ oligodendrocytes gradually increased during the examined period, P8–P18, in both genotypes (Fig. 5*A*). In *Cntn1*-KO nerves a lower proportion of oligodendrocytes matured on time in comparison with WT. Specifically, in *Cntn1*-KO vs. WT optic nerves, APC^+ cells were reduced by 19% at P8, 31% at P11 ($P < 0.05$), and 19% at P15. By P17–18, the difference between KO and WT APC^+ cells was at a modest 10%. Triple labeling for APC, NG2, and DAPI at P18 showed that 10%

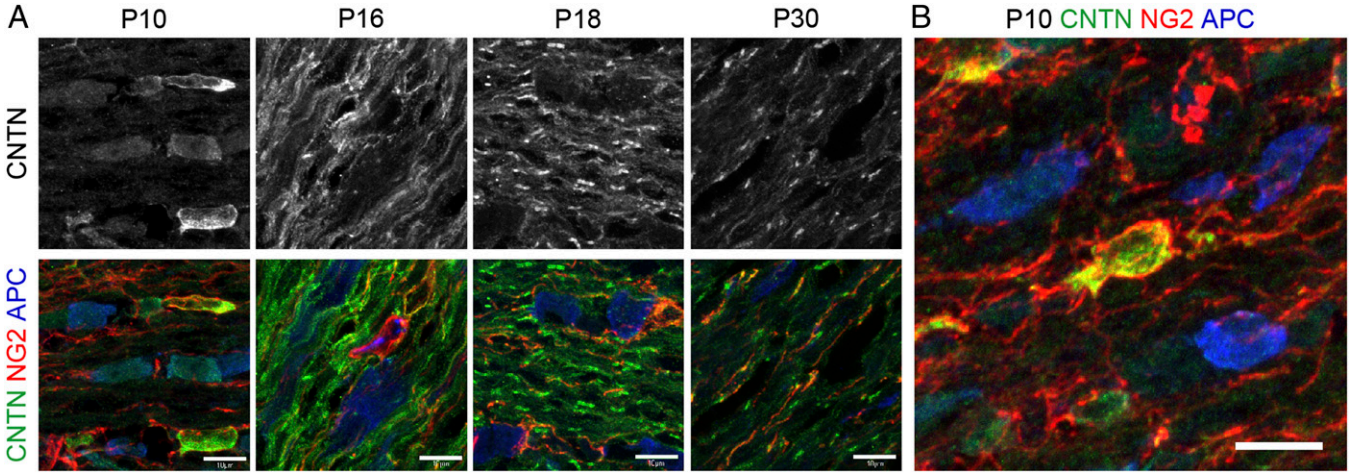

Fig. 2. Contactin expression by oligodendrocyte progenitor cells and down-regulation from mature myelin. Optic nerves from WT mice were fixed with 4% PFA and stained for Contactin and early and late markers for oligodendrocytes, NG2 and APC, respectively. (*A* and *B*) At P10, Contactin expression is polarized in $NG2^+$ cells, and is low on APC^+ cells. (*A*) At P16, Contactin is mostly present on loose membranes and at few paranodes. At P18, Contactin is clearly observed at most paranodes, some nodes, and on loose membranes. By P30, Contactin overall expression is lower, and observed at nodes (3-h fixation, −MOH) and at low levels on loose membranes. (Scale bars, 10 μm.)

increase in the number of $NG2^+$ OPCs made up for the decrease in APC^+ oligodendrocytes in *Cntn1*-KO nerves (Fig. 5*B*). These data suggest a transient delay in oligodendrocyte development in *Cntn1*-KO mice that is at a modest 10% at the P18 experimental endpoint.

Because the decrease in the number of mature oligodendrocytes insufficiently explains the significant myelin loss in *Cntn1*-KO optic nerves, we searched for alternative mechanisms. In vitro experiments have implicated Contactin-mediated signals in triggering events that lead to myelin membrane expansion (18, 19). To address if loss of Contactin affected the extension of oligodendrocyte membranes, we generated *Cntn1*-KO and WT littermate mice expressing GFP in the oligodendrocyte lineage. Transgenic mice expressing GFP from the proteolipid (PLP) promoter (24) were crossed with *Cntn*1-KO mice to demarcate oligodendrocytes and their processes during myelination. Transgenically expressed PLP-GFP is reported to diffuse into oligodendrocyte processes that wrap axons marking the myelin segments (25). In P18 optic nerves, a similar proportion of cells expressed PLP-GFP in cell somata in both genotypes (WT: 18% and KO: 20% of all $DAPI^+$ cells, $P = 0.74$, $n = 3$). We used the amount of GFP fluorescence in P18 WT and *Cntn1*-KO optic nerves as a measure for oligodendrocyte membrane extension. Oligodendrocytes in *Cntn1*-KO mice were significantly impaired in their ability to extend and wrap myelin membrane around axons. In Fig. 5*C*, we illustrate the decrease of GFP^+ oligodendroglial processes in *Cntn1*-KO vs. WT optic nerves. Quantitative measurement of GFP fluorescence intensity in equally sized optic fields using ImageJ revealed 46% reduction in knockout oligodendrocyte processes (Fig. 5*D*) ($P < 0.05$). Confirming that PLP-GFP expression extends into myelin processes, the GFP-marker was detected on internodes labeled for myelin markers MBP and

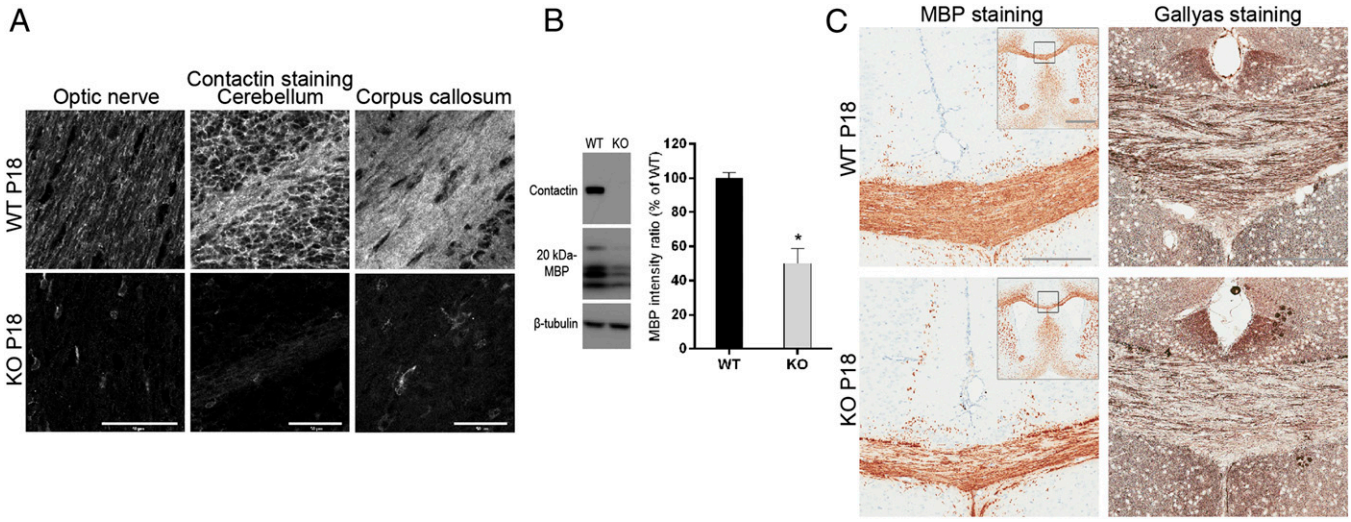

Fig. 3. Decreased myelin formation in *Cntn1*-KO mice. (*A*) Immunohistochemisty for Contactin on P18 WT or *Cntn1*-KO (KO) optic nerve, cerebellum, and corpus callosum. Contactin was abolished in KO samples. (Scale bars, 50 μm.) (*B*) Western blotting of whole-brain samples from P18 WT and KO mice documents the absence of Contactin and ∼50% reduction of MBP in KO samples (levels normalized to β-tubulin, $*P < 0.05$, $n = 3$). (*C*) MBP and myelin (Gallyas) staining of P18 samples shows reduced levels on KO corpus callosum compared with WT. Squares in *Insets* for MBP staining show the positions of magnified images. (Scale bars, 200 μm; *Inset*, 1 mm.)

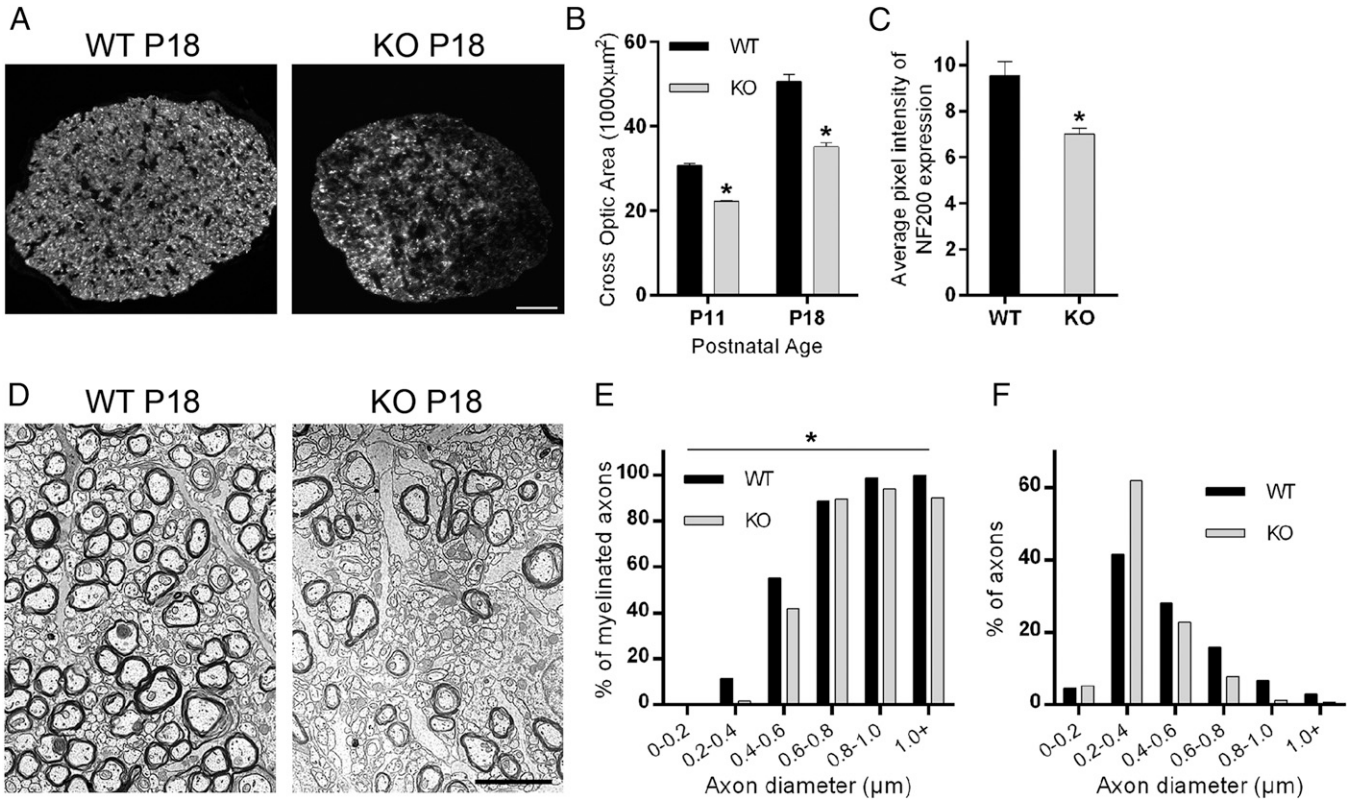

Fig. 4. Contactin regulates optic nerve thickness and myelin development. (*A*) Contactin WT and KO optic nerve cross sections were stained for NF200 at P18. (Scale bar, 30 μm.) (*B*) Contactin deficiency resulted in reduced optic nerve thickness compared with WT at P11 (*$P < 0.01$, $n = 4$) and P18 (*$P < 0.01$, $n = 4$). (*C*) *Cntn1*-KO nerves had reduced NF200 expression compared with WT at the same age (*$P = 0.01$, $n = 4$). (*D*) Electron micrographs show 60% reduction in numbers of myelinated axons and increased numbers of small-diameter axons in KO samples compared with WT at P16 (see text for details). (Scale bar, 2.5 μm.) (*E*) The graph shows percentage of myelinated axons according to axon diameter for KO and WT mice. In the KO condition, reduced myelination was most evident for axons with diameters less than 0.6 μm. (*F*) Analyses of axon diameters revealed an increased ratio of small-diameter axons (0.2–0.4 μm) and reduced ratios for larger-diameter axons for KO. Quantification for *E* and *F* was performed with more than 1,000 axons per genotype. The overall difference between WT and KO by two-way ANOVA was significant for *E* (*$P < 0.05$) but not significant for *F* ($P > 0.05$).

MOG (myelin-oligodendrocyte glycoprotein) (Fig. 5 *E* and *G*). Moreover, PLP-GFP highly accumulated at paranodal regions identified by Caspr staining (Fig. 5*F*). Quantitative reduction of PLP-GFP expression in *Cntn1*-KO optic nerve strongly suggests that Contactin-mediated signals are required for myelin membrane expansion that is prerequisite for proper myelination.

Disrupted Paranodal Junctions in *Cntn1*-KO Central Myelin. Despite impairments in oligodendrocyte membrane expansion, some axons in *Cntn1*-KO optic nerves were still encircled with myelin. As Contactin regulates the paranodal assembly in the PNS (12), we examined the domain organization of P17 WT and *Cntn1*-KO myelinated optic nerves. Nodes of Ranvier, identified with pan-sodium channel antibodies, were flanked by Caspr- and Contactin-positive paranodal junctions in WT nerves. (Fig. 6 *A* and *B*). In the *Cntn1*-KO condition, Caspr expression was completely abolished from the axon membrane (Fig. 6*A*), and instead resided in the cell bodies of retinal ganglion cells (RGC). Thus, Contactin, in CNS like in PNS, regulates Caspr expression on the axon membrane.

To further evaluate the axonal domains around the node, we probed the location of the $K_v1.2$ shaker-type voltage-gated potassium channel subunits that normally concentrate at the juxtaparanodal region adjacent to the paranodes (26). In WT optic nerves, paranodal gaps segregated the sodium channel clusters at the nodes from the potassium channels located just under the myelin (Fig. 6*A*). In contrast, in *Cntn1*-KO nerves, $K_v1.2$ channels were mislocalized to positions adjacent to the nodes (Fig. 6*A*).

To evaluate the organization of disrupted paranodes in *Cntn1*-KO mice at the ultrastructural level, we examined longitudinally sectioned P16 optic nerves by electron microscopy. WT nerves showed normal paranodal junctions with attachment sites characterized by the transverse, electron-dense bands, and the outermost myelin loops closest to the nodes (Fig. 6*C*, WT paranode). In contrast, paranodal junctions in *Cntn1*-KO nerves were severely disrupted (Fig. 6*C*, KO paranode). Most of the mutant terminal myelin loops displayed overt disorganization with various cellular phenotypes, including astrocytic processes penetrating between the axon and paranodal glial membranes (Fig. 6*C*, red structures, *Middle*), or abnormally structured, everted, and smaller myelin loops (Fig. 6*C*, blue structures, *Bottom*). None of the paranodal structures in *Cntn1*-KO optic nerves showed junctional attachment characterized by the electron-dense transverse bands (Fig. 6*C*). Evaluating the frequency of nodal structures bilaterally flanked by myelin terminal membranes, regardless of appearance, revealed an ~60% reduction in the KO condition. Only 13 of 42 nodal regions (31%, $n = 3$) were surrounded by myelin in *Cntn1*-KO compared with 13 of 17 (76%, $n = 3$) in WT nerves (Fig. 6*D*). Most of the terminal myelin loops in *Cntn1*-KO nerves turned away from the axon membrane, and only 20% showed axonal orientation (Fig. 6*E*). These phenotypes support an essential role for Contactin in the formation of the septate-like axoglial junctions in the CNS, by mechanisms previously established for the PNS (12).

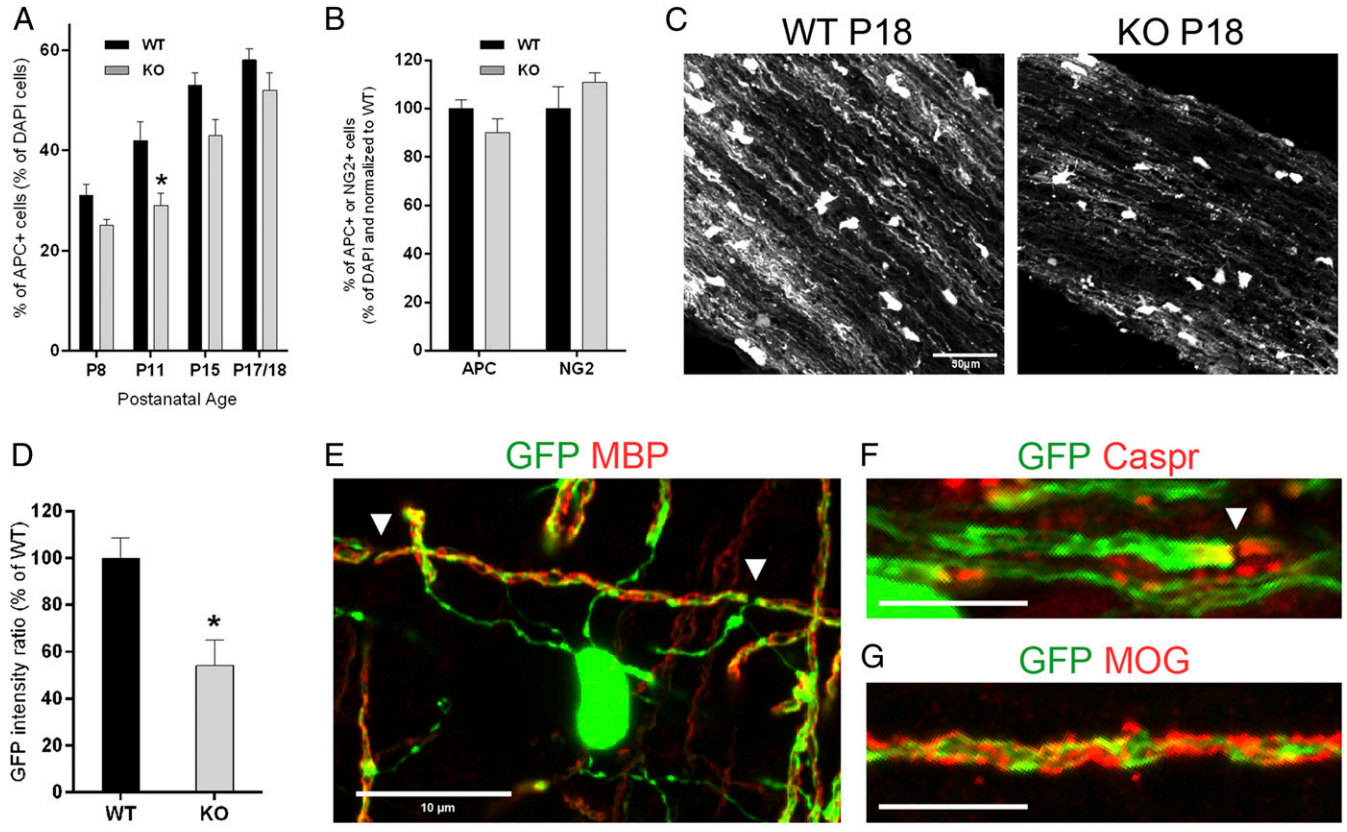

Fig. 5. Impaired oligodendrocyte differentiation and myelin membrane expansion in *Cntn1*-KO optic nerves. (*A* and *B*) Oligodendrocyte maturation in WT and KO optic nerves was assessed by APC and NG2 immunostaining. (*A*) The graph shows the percentage of $APC^+/DAPI^+$ cells from P8 to P18 (P8, $P = 0.08$; P11, $^*P < 0.05$; P15, $P = 0.11$, $n = 3$ for each condition; P17/18, $P = 0.16$, WT $n = 10$, KO $n = 6$). (*B*) The graph shows the percentage of APC^+ and $NG2^+$ cells normalized to WT levels at P17/18 (APC, $P = 0.16$, WT $n = 10$, KO $n = 6$; NG2, $P = 0.45$, $n = 3$). (*C*) Myelin membrane expansion was detected by GFP expression from the PLP promoter. (Scale bar, 50 μm.) (*D*) GFP fluorescence was reduced by ∼46% in *Cntn1-KO* compared with WT optic nerves at P18 ($^*P < 0.05$, $n = 4$). (*E*) GFP signal colocalizes at myelin segments stained with MBP, demarcated by arrowheads. (*F*) GFP accumulates at paranodal regions, here marked with Caspr staining (arrowhead). (*G*) GFP signal distribution at myelin segments is also shown with MOG staining. (Scale bars in *E*–*G*, 10 μm.)

The ∼60% reduction in the frequency of nodes with bilateral myelin loops is specific to the *Cntn1*-KO CNS and reflects the significant myelin loss that is not observed in the PNS of *Cntn1* mutants.

Decreased Frequency and Delayed Maturation of Nodal Sodium Channels in *Cntn1*-KO Optic Nerves. Two major pore-forming sodium channel α-subunits regulate the electrophysiological properties of the postnatal optic nerve. $Na_v1.2$ subunits define the nodes and the axon initial segment during early postnatal development and the progressive switch from $Na_v1.2$ to $Na_v1.6$ channel subtypes around P16 establishes mature channel properties and conduction characteristics of adult myelinated optic nerves (27, 28). To determine if the Contactin mutation affected the number of nodal sodium channel clusters in P16 optic nerves, we counted clusters immunostained with a pan-sodium channel antibody. The number of sodium channel clusters was reduced by 65% in *Cntn1*-KO nerves compared with equally sized and positioned areas in WT (Fig. 7 *A* and *B*). Many of the existing clusters in *Cntn1*-KO nerves were highly distorted in shape and size. Common patterns were the appearance of thinning streaks along the axon, clusters gradually decreasing in intensity toward the extremes, and elongated clusters. Immunohistochemistry for sodium channel-associated Ankyrin-G confirmed this phenotype.

To address if the *Cntn1*-KO mutation affected the developmental switch of sodium channel subtypes, we examined $Na_v1.6$ in combination with the pan-sodium channel marker by immunohistochemistry. We found a significant reduction of $Na_v1.6$ in *Cntn1*-KO optic nerves (Fig. 7 *A* and *C*). In WT mice, 78% of all nodes expressed $Na_v1.6$, whereas only 45% displayed $Na_v1.6$ in mutant nerves (Fig. 7*C*). Taking these data together, ∼65% fewer sodium channel clusters formed in *Cntn1*-KO compared with WT optic nerves, and of those only 45% matured to express the $Na_v1.6$ channel subtype. This result constitutes a severe impairment, with an ∼80% reduction in the number of mature $Na_v1.6$ expressing nodes in *Cntn1*-KO optic nerves at the experimental endpoint.

Discussion

Multiple signals regulate interactions between axons and oligodendrocytes during myelination. We here report critical roles for Contactin in early and late steps of axon–glia communication in developing myelin. In postnatal optic nerves, Contactin is necessary for early interactions between axons and glia to regulate axon maturation and effective expansion of oligodendrocyte membranes. Later, Contactin orchestrates assembly of paranodal axoglial junctions, and regulates formation and maturation of nodes that establish the domain organization necessary for functional properties of myelinated nerves. Contactin is dynamically expressed on axons and oligodendrocytes during myelination and is essential for CNS myelination.

Contactin in Axon–Glia Interactions Initiating Myelin Formation. Myelination occurs in distinct stages during which OPCs migrate from their sources of origin to proliferate and populate nerves before myelinating selected axon populations. Contactin-

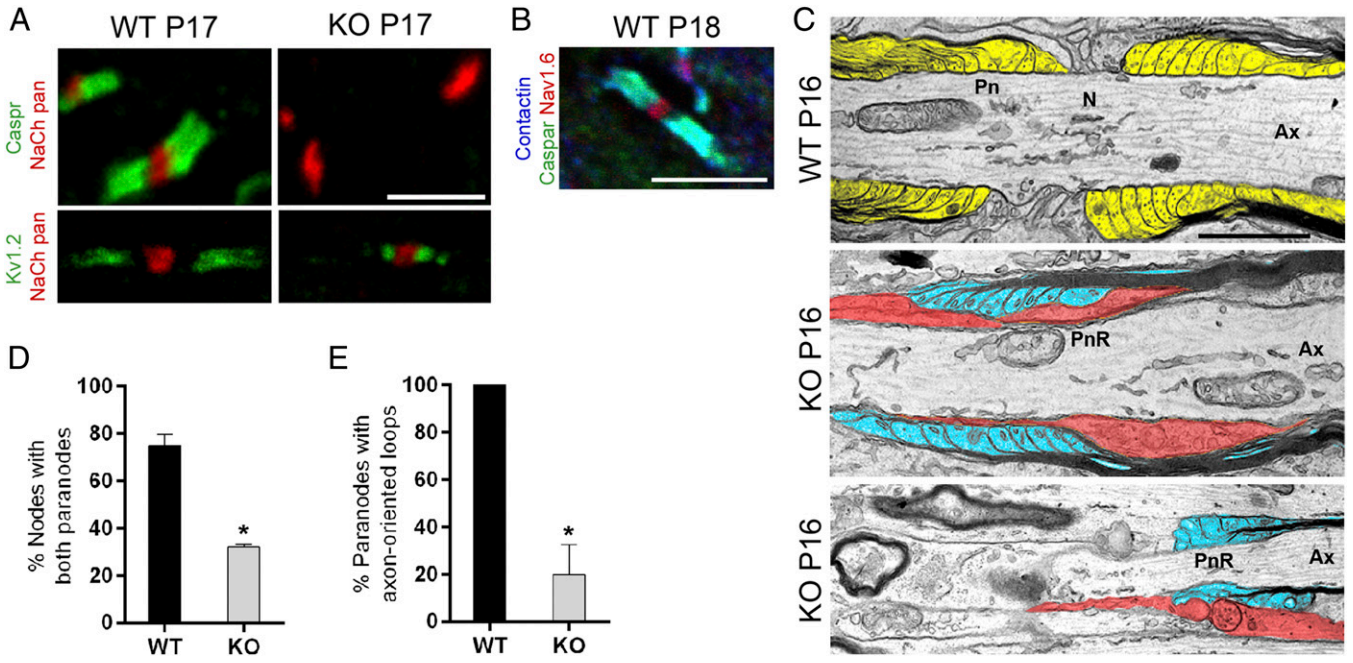

Fig. 6. Disrupted paranodal junctions in *Cntn1*-KO central myelin. (*A*) Contactin deficiency (KO) resulted in paranodal defects. In WT axons, Caspr (green) was expressed at paranodes. Nodes were identified with pan-sodium channel antibody (red). In the KO condition, Caspr was abolished from axons. (*Lower*) Potassium channel $K_v1.2$ expression (green) at the juxtaparanodes in WT. In KO, $K_v1.2$ was mislocalized adjacent to nodal sodium channel clusters (red). (*B*) In WT nerves, Contactin (blue) colocalized with Caspr (green) at the paranodes, adjacent to nodes expressing $Na_v1.6$ (red). (Scale bars, 5 μm.) (*C*) Electron micrographs from P16 WT optic nerves showed well-organized myelin loops and paranodal attachments (pseudocolored in yellow). KO nerves displayed severely disrupted paranodes characterized by loss of attachment sites, averted myelin loops (pseudocolored in blue), or cellular processes (pseudocolored in red), penetrating between the axonal and glial membranes in the paranodal region (PnR) (Ax, axon; N, node; Pn, paranode). (Scale bar, 1 μm.) (*D*) Number of nodes with double paranodes was reduced to 31% in KO compared with 76% in WT (*$P < 0.05$, $n = 3$). (*E*) Of all paranodes, only 20% in KO showed paranodes with axon-oriented loops (*$P < 0.05$, $n = 3$).

mediated signals impact the latter stage when oligodendrocytes differentiate into myelinating cells and expand the membrane to enwrap axons. Comparable numbers of oligodendrocyte lineage cells were present in *Cntn1*-KO and WT optic nerves, indicating that Contactin has no overt impact on cell proliferation and migration in vivo. The Contactin null mutation, however, significantly restricted oligodendrocytes from forming myelin membrane around axons. Multiple approaches, biochemistry, histology, transgenic GFP expression in oligodendrocytes, and electron microscopy consistently showed ∼50% reduction of myelin in *Cntn1*-KO mice. Thus, analyses of *Cntn1*-KO mice document a critical role for Contactin in CNS myelination.

Investigating oligodendrocytes, we found that comparable numbers reached position in optic nerves in both genotypes, and all but 10% of OPCs matured into APC^+ cells in *Cntn1*-KO mice at the P18 experimental endpoint. Contactin-deficient oligodendrocytes, however, extended 50% less membrane than their WT counterparts. Taken in isolation, this result is consistent with in vitro studies documenting that Contactin on oligodendrocytes promotes myelin membrane generation (18). The proposed model is that engagement of glial Contactin activates Src-related intracellular kinase Fyn to induce transport and local translation of MBP mRNA at oligodendrocyte processes increasing membrane expansion (18, 29). Consistent with this model, *Cntn1*-KO mice show hypomyelination and overall MBP reduction in multiple myelinated areas of the CNS, similar to the phenotype in Fyn-deficient mice (30).

However, additional parameters play into the *Cntn1*-KO hypomyelination phenotype. In optic nerves, axons extended by RGCs display different sizes and conduction velocities with mostly the larger-diameter axons encircled by myelin (31). *Cntn1*-KO optic nerves show a prevailing number of small, immature fibers, as judged by ultrastructure and reduced NF200 expression (22, 23). This finding indicates a defect in axon maturation, which is a critical parameter for myelination. Axon development depends on three major parameters: target innervation, intrinsic factors, and signals from oligodendrocytes. Because initial analyses of P18 mice did not reveal overt abnormalities of labeled RGC axons reaching the lateral geniculate nucleus target, the axon defects in *Cntn1*-KO mice are likely intrinsic or a result of disrupted axon-oligodendrocyte communication. To gain further insights, we scored myelinated RGC axons by diameter and genotype. Overall, significantly fewer axons were myelinated in *Cntn1*-KO mice, with prevailing differences in myelination of the small-diameter axons (0.2–0.6 μm).

Several interpretations may apply to this phenotype. First, neuronal Contactin may be necessary for axon maturation. Contactin interactions with any or several of neuronal cell-surface proteins, including L1/NgCAM, RPTPα, NrCAM, neurofascin, and sodium channel-β1, may affect cellular mechanisms required for axon maturation (16, 32–35). Second, as numbers of oligodendrocytes in optic nerves are comparable between genotypes, in *Cntn1*-KO the number of oligodendrocytes may be insufficient to match the demand of myelinating an increased number of small-diameter axons. Third, as the myelination defect in *Cntn1*-KO optic nerves was most evident for smaller-diameter axons (<0.6 μm), we could argue that these axons are impaired in glial signaling and recruitment. Immature axons in *Cntn1*-KO nerves may not provide oligodendrocytes with sufficient molecular, contact-, or activity-mediated signals for axon maturation and myelination (36, 37). Larger-diameter axons may overcome this limitation by producing signals above threshold and higher electrical activity. Finally, axon maturation is regulated by signals from oligodendrocytes (38–42). Glial Contactin could influence

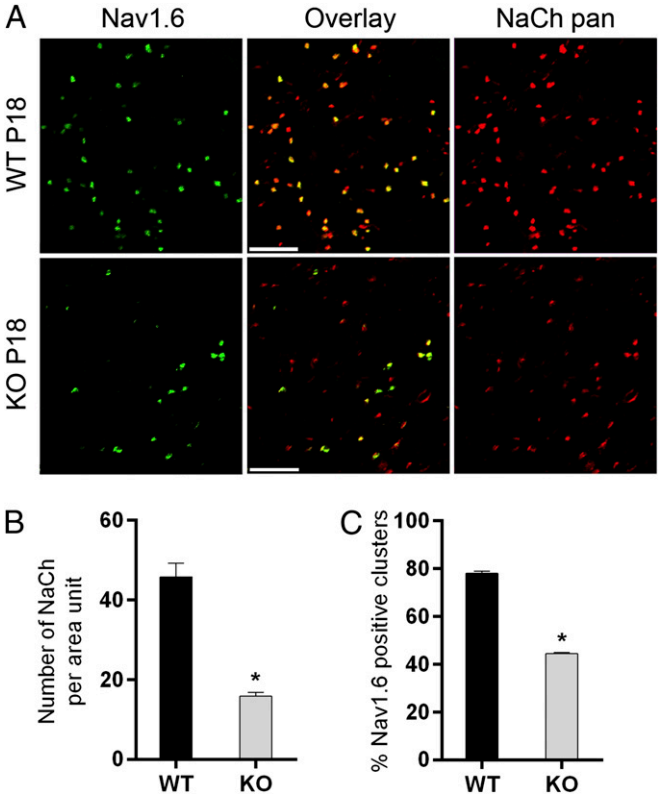

Fig. 7. Contactin regulates nodal sodium channel development. Sodium channel clustering in the optic nerve was disturbed in *Cntn1*-KO at P18. (*A*) WT and KO optic nerve sections were stained for $Na_v1.6$ (green) and NaCh pan (red). Fewer total number of nodes (red images compared), fewer mature nodes (green images compared), and more elongated sodium channel clusters (red images compared) were observed on KO compared with WT. (Scale bar, 5 μm.) (*B*) Quantification shows reduced number of NaCh clusters per area unit in *Cntn1*-KO compared with WT (*$P < 0.005$ WT $n = 5$, KO $n = 4$). (*C*) KO samples contain reduced number of sodium channel clusters expressing $Na_v1.6$ (*$P < 0.005$ WT $n = 5$, KO $n = 4$).

axon maturation and diameter, which in turn is necessary to provide signals for myelination (36, 37). The fact that mainly smaller axons remain unmyelinated in *Cntn1*-KO nerves may indicate that glial Contactin, in addition to regulating myelin membrane extension, may be important to sense axon size to initiate myelination. A shift in the threshold diameter for myelination was suggested for integrins, and Contactin associates with integrin α6β1 on oligodendrocytes (19, 43). Although our analyses in mice systemically deficient for Contactin cannot distinguish between these possibilities, our data clearly show that Contactin is necessary for proper communication between axons and oligodendrocytes during myelin formation in the CNS.

Contactin in Domain Organization of Myelinated Central Nerves.

Paranodal assembly. Prominent Contactin at nodes and paranodes suggests roles for Contactin in the domain organization of myelinated nerves. Similar to the periphery (12), in *Cntn1*-KO CNS we observed disrupted paranodal junctions characterized by loss of Caspr and mislocalization of the shaker-type potassium $K_v1.2$ channels that normally define juxtaparanodal regions (1, 26). These defects parallel the paranodal deficiencies in Caspr- and UDP-galactose:ceramide galactosyltransferase (CGT)-KO mice, and indicate complete loss of paranodal functions as diffusion barriers for voltage-gated Na_v and K_v channels (44–46). Several studies queried if paranodal assembly is necessary for myelination. In peripheral myelin, only neurons express and selectively accumulate Contactin at paranodal axon membranes. Peripheral myelinating glia (Schwann cells) do not express Contactin and form normal-looking myelin without paranodal axon contact in *Cntn1*-KO mice (12). Mice with paranodal defects, such as Caspr- and CGT-KO mutants, show no major impairments of myelin loss in the PNS and CNS, indicating that disrupted paranodes are impartial to myelin formation (45, 47, 48). In the Caspr-KO background, even additional mutations in axonal cytoskeletal scaffold protein βIV-spectrin, or in nodal extracellular matrix (ECM) proteins, leave CNS myelination relatively unaffected (48). We therefore consider the paranodal defects in *Cntn1*-KO CNS independent from the hypomyelination phenotype. Combined with our previous work, the current data establish that Contactin regulates paranodal domain organization in both CNS and PNS.

Formation and maturation of nodal sodium channel clusters. In the CNS, nodes assemble after paranodal formation and are stabilized through ECM and cytoskeletal interactions (27, 48, 49). Node formation is severely reduced in *Cntn1*-KO mice, and the remaining nodes display abnormal shapes and impaired maturation. A recent study by Susuki et al. documented multiple orchestrating mechanisms in regulation of nodal assembly and stabilization (48). Based on our data, we propose that a single molecule, Contactin, can impact node formation by multiple mechanisms.

First, Contactin is important for efficient expansion of oligodendrocyte membranes that engage with axons and form axoglial junctions. Impaired oligodendrocyte membrane extension, as observed in *Cntn1*-KO mice, reduces the frequency of axonal contacts and yields fewer nodes.

Second, Contactin is essential for paranode formation, which regulates CNS nodal assembly. Paranodal junctions form as oligodendrocyte processes enwrap axons with myelin. Terminal loops of each myelin segment anchor to axonal membrane and cluster sodium channels in front of the internode and potassium channels underneath. Disruption of paranodes, as in Caspr- and CGT-KO mice, does not drastically reduce nodal numbers but distorts their shapes and maturation. This finding suggests that paranodes regulate tightness and maturation, but not the frequency of nodal clusters (45, 46, 48–50). Nodal numbers are significantly reduced in the Caspr-KO background only in combination with additional mutations: disrupted βIV-spectrin, which anchors sodium channels to the cytoskeleton, or ECM proteins that stabilize the nodes extracellularly (48). The parallel defects in *Cntn1*-KO mice with this latter phenotype raise the possibility that axonal Contactin, in addition to its role at paranodes, participates in stabilizing nodal complexes through NF186 or ECM interactions. Indeed, several studies documented Contactin interactions with various cytoskeleton-associated membrane proteins and ECM components, including neurofascins, NgCAM, NrCAM, RPTP-β/phosphacan, tenascin-R, and tenascin-C (32–34, 51–53).

Third, Contactin directly associates with sodium channel-β1 subunits to increase channel surface expression and current density in vitro (16, 54, 55). Contactin deficiency could thus limit the number of sodium channels on axon surfaces, and thereby decrease neuronal activity, which is crucial for myelination and oligodendrocyte differentiation in vitro and in vivo (56–59). Indeed, Kazarinova-Noyes and Shrager recorded reduced compound action potential velocity in *Cntn1*-KO optic nerves (60). In *Cntn1*-KO nerves, diminished nerve activity could impact signals for initiating myelination by resident oligodendrocytes, and reduce subsequent paranode- and node formation. We conclude that loss of Contactin-mediated communication between axons and oligodendrocytes reduces myelin and nodal frequency and that simultaneous disruption of paranodes impairs nodal shapes and maturation.

In summary, our work supports the model that Contactin regulates multiple aspects of axon–glia interactions during CNS

myelination. Contactin contributes early signals to regulate axon maturation, extension of oligodendrocyte membranes, and initiation of myelination, which determines the frequency of initial axoglial contact and amount of myelin formation. At later stages, Contactin regulates domain organization of myelinated nerves by orchestrating the formation of paranodal axoglial junctions that critically determine the properties of myelinated nerves. Disruption of these events during brain injury and demyelinating diseases, such as in multiple sclerosis, contributes to severe neurological deficits. Identification of Contactin's key contribution adds novel molecular understanding to CNS myelination and may guide future studies toward regeneration in the diseased brain. It is now critical to determine the specific molecular mechanisms by which Contactin regulates the remarkable cellular assembly that constitutes myelin, and evaluate its potential for myelin repair in the CNS.

Materials and Methods

Mice. All experiments were approved by the Institutional Animal Care and Use Committee of Sanford-Burnham Medical Research Institute (La Jolla, CA). The derivation of mice homozygous for the mutant *Contactin-1* (*Cntn1*) allele was described previously (10). Transgenic mice expressing GFP from the proteolipid promoter (*PLP-GFP*) were intercrossed with heterozygous *Cntn1*-KO mice to create homozygous *Cntn1*-KO and WT progeny expressing GFP in the oligodendrocyte lineage. *PLP-GFP* mice were provided by Wendy Macklin (University of Colorado at Denver, Denver, CO) (25) and obtained through Biogen Idec. In this study, WT mice were analyzed at P10–30. Homozygous *Cntn1*-KO mice survive up to P18 (10) and were compared with WT littermates between P10 and P18.

Immunostaining. For optimizing Contactin staining, optic nerves were drop-fixed in 4% (wt/vol) PFA for 10 min to 5 h before processing. Alternatively, nerve tissue was treated with 100% ice-cold methanol for 10 min after 4% PFA fixation. Optic nerves were cryosectioned at 6-μm thickness. Brains were dissected from mice perfused with 4% PFA and postfixed in 4% PFA for 1–5 h. Fixed tissues were cryoprotected in 30% sucrose in PBS (pH 7.4) overnight at 4 °C, embedded and frozen in OCT compound (Sakura), and cryosectioned at 30-μm thickness (Leica CM 3050 S). Floating sections were collected in PBS.

Contactin staining. Tissue sections were sequentially incubated in 1% glycine for 15 min and blocking solution (5% BSA, 2% normal donkey serum, 0.2% Triton X-100) for 1 h. Rabbit- [1:1,000 (10)] or goat anti-Contactin, antibodies (Neuromics; 1:1,000) in Dako Antibody Diluent were bound overnight at 4 °C. Following washes in PBS and blocking in PBS containing 5% normal donkey serum and 0.5% Triton X-100, sections were incubated with Alexa-conjugated secondary antibodies (Molecular Probes) in Dako solution. After final washes, sections were mounted using Dako Cytomation fluorescent mounting medium. Data were collected using Fluoview 1000 Olympus Laser Point Scanning Confocal or TE300 Nikon Wide Field Fluorescence Microscope.

Antibodies. Rabbit anti-NG2 (1:1,000; a gift from Bill Stallcup, Sanford-Burnham Medical Research Institution, La Jolla, CA), mouse anti-APC (CC-1, 1:100; Calbiochem; or Ab-7, 1:20; Oncogene), mouse antisodium channel (pan, K58/35, 1:800; Sigma), mouse anti-Kv1.2 (1:200; Upstate Biotechnology), rabbit antisodium channel (loop III-IV, 1:100; Upstate Biotechnology), rabbit anti-$Na_v1.6$ (1:400; a gift from Matthew Rasband, Baylor College, Houston), mouse anti-$Na_v1.2$ (K69/3, 1:600; gift from Matthew Rasband), goat anti-MOG (1:250; R&D Systems), and mouse anti–Ankyrin-G (33-8800, 1:100; Zymed). For Caspr, bivalent Fab miniantibodies, dimerized via helix-turn-helix motif and tagged with a myc- and his-tag, were isolated from the Human Combinatorial Antibody Library (HuCAL) GOLD (61) in collaboration with AbD Serotec by their ability to bind recombinant rat Caspr glutathione fusion protein representing the cytoplasmic domain (clone AbD06152, product code HCA091). Antibodies were validated for detecting Caspr in brain sections. Rabbit anti-Caspr antibody (1:1,000; a gift from Elior Peles, Weizmann Institute, Rehovot, Israel) confirmed specificity, and was used in some of the initial experiments. DAPI (Molecular Probes) was used as a counterstain for cell nuclei.

MBP and Gallyas Staining. For immunohistochemical detection of MBP (SMI-94, 1:1,000; Covance), we applied the Avidin-Biotin Peroxidase Complex (ABC) procedure on paraffin sections. Sections were deparaffinized, equilibrated in PBS, and incubated in primary antibody solution in 5% normal serum, 0.3% Triton X-100 in PBS overnight at 4 °C. Following PBS washes, biotinylated horse anti-mouse secondary antibodies (1:200; Vector) were applied. Antibody signal was detected using ABC (Vector) and DAB solutions (Sigma). Staining was intensified by treating sections with 0.05% OsO_4 for 15–30 s.

Gallyas silver staining was used to detect the myelin (62). Briefly, deparaffinized sections were treated with Pyridine:Acetic anhydride solution for 45–60 min, 50% ethanol for 3 min, 25% ethanol for 3 min, 0.05% acetic acid for 2.5 min, 0.1% acetic acid for 2.5 min, and 0.5% acetic acid for 10 min. Then, sections were incubated in silver nitrate solution for ∼1 h and 0.5% acetic acid for 10 min. The final steps included treatment with ABC solution for 4–5 min, 0.5% acetic acid for a min, 0.2% potassium ferricyanide for 5–10 min, ddH_2O for 1 min, 0.5% sodium thiosulfate for 1–3 min, and washing twice in ddH_2O for 4 min. The final steps were repeated three times before sections were washed in ddH_2O for 5 min. After standard dehydration, coverslips were mounted. Sections were imaged using the Aperio Virtual slide imaging ScanScope XT system.

Western Blotting. Whole mouse brains were homogenized with Teflon-glass homogenizer in ice-cold RIPA buffer in the presence of protease inhibitors (Complete Mini; Roche). The homogenates were centrifuged at 15,000 × *g* for 30 min at 4 °C, and protein concentrations of supernatants were determined using Dc-Protein Assay (Bio-Rad). Samples were heated at 100 °C for 10 min and centrifuged before loading onto SDS/PAGE gels (Novex 4–20% Tris·Glycine Gel; Life Technologies). Separated proteins were transferred to PVDF membrane (Immobilon-P, pore size 0.45 μm; Millipore) and processed for immunoblotting with primary antibodies: goat anti-Contactin (1:1,000; R&D), mouse anti-MBP (SMI-94, 1:1,000), and mouse anti–β-tubulin (MAB3408, 1:5,000; Millipore). Secondary antibodies were HRP-conjugated goat anti-mouse or rabbit anti-goat IgG (ECL, GE Healthcare). The HRP signal was detected using Amersham ECL Western Blotting Detection Reagents (GE Healthcare), and scanned to digitize. Data were quantified using ImageJ Gel Analysis tool (http://imagej.nih.gov/ij/), and the MBP signal was normalized to β-tubulin levels.

Standard Electron Microscopy. Sample preparation was previously described (63). Optic nerves were sectioned either longitudinally for examining the paranodes, or transversely to monitor myelin structure. Ultrathin sections were collected on 200-mesh grids, and photographed under a Hitachi 600 electron microscope.

Quantitative Analyses. ***Oligodendrocyte maturation.*** Quantification of DAPI, GFP^+, APC^+, and $NG2^+$ cells was performed using ImagePro Plus software (MediaCybernetics). Three identical regions (AOI) were selected on every image. After background subtraction, images were converted to binary format using the threshold function (threshold values were kept constant for the same markers). Cell bodies were identified using the "count/size" function and were manually split or merged.

Paranodes and myelin. Electron micrographs of nodes of Ranvier were taken from longitudinally sectioned optic nerves at 15,000× magnification, scanned, and digitized in ImageJ. For myelin quantification, electron micrographs were taken at the center of each nerve at 3,000× magnification, scanned, and digitized in ImageJ. Dense myelin was evident as thick multilayered membrane around axons. Axons were manually labeled using ImageJ to quantify their areas, which were used to calculate axon diameters. We counted more than 1,000 axons from two mice per genotype from nonoverlapping randomly chosen areas. After scoring the axons as myelinated or unmyelinated, the percentage of myelinated axons was determined. The *P* value was calculated with a two-way ANOVA test.

Sodium channels. Quantification of $Na_v1.6$ /NaCh pan and NaCh pan clusters was performed using confocal images. All images were merged and processed with Photoshop 7.0 software. The relative amount of $Na_v1.6$ channel clusters was derived from the total number of $Na_v1.6$/Pan-sodium channel-positive nodes divided by total number of nodes labeled for the pan-sodium channel.

ACKNOWLEDGMENTS. We thank Dr. Edward Monosov for providing his expertise in Cell Imaging; Agniezska Brzozowska-Prechtl and Robbin Newlin for performing the paraffin histology; Daren Ginete and Kathrin Keune for assisting with genotyping; Adriana Charbono and Francisco Beltran for expert care of the mutant mice; Dr. Wendy Macklin (University of Colorado, Denver) for generously providing the proteolipid promoter-GFP mice; Dr. Andrew Huberman (University of California, San Diego) for allowing mention of his preliminary work on retinal ganglion cell projections in *Cntn1*-KO mice; Dr. William B. Stallcup (Sanford-Burnham Medical Research Institute) for providing rabbit NG2 antibody; Dr. Matthew Rasband (Baylor College of Medicine) for providing sodium channel antibodies; and Dr. Elior Peles (Weizmann Institute) and AbD Serotec for providing the rabbit and human Fab miniantibodies, respectively, against Caspr.

U.B.-T. conducted this work as part of the requirements for a doctoral degree from the Karolinska Institutet, Stockholm, Sweden, under supervision of Prof. Martin Schalling and Dr. Jeanette Johansen, Department of Molecular Medicine and Surgery, Center for Molecular Medicine. This project was supported by National Multiple Sclerosis Society Grant RG-4666-A-2 (to B.R.) with support for preliminary work from National Institutes of Health Grant RO1 NS038297 (to B.R.) and a fellowship from the Sweden-America Foundation (to U.B.-T.).

1. Baumann N, Pham-Dinh D (2001) Biology of oligodendrocyte and myelin in the mammalian central nervous system. *Physiol Rev* 81(2):871–927.
2. Nave KA (2010) Myelination and support of axonal integrity by glia. *Nature* 468(7321): 244–252.
3. Miller RH (2002) Regulation of oligodendrocyte development in the vertebrate CNS. *Prog Neurobiol* 67(6):451–467.
4. Sherman DL, Brophy PJ (2005) Mechanisms of axon ensheathment and myelin growth. *Nat Rev Neurosci* 6(9):683–690.
5. Dutta R, Trapp BD (2011) Mechanisms of neuronal dysfunction and degeneration in multiple sclerosis. *Prog Neurobiol* 93(1):1–12.
6. Ben-Hur T, Goldman SA (2008) Prospects of cell therapy for disorders of myelin. *Ann N Y Acad Sci* 1142(1):218–249.
7. Franklin RJ, Ffrench-Constant C (2008) Remyelination in the CNS: From biology to therapy. *Nat Rev Neurosci* 9(11):839–855.
8. Ranscht B (1988) Sequence of contactin, a 130-kD glycoprotein concentrated in areas of interneuronal contact, defines a new member of the immunoglobulin supergene family in the nervous system. *J Cell Biol* 107(4):1561–1573.
9. Gennarini G, Cibelli G, Rougon G, Mattei MG, Goridis C (1989) The mouse neuronal cell surface protein F3: A phosphatidylinositol-anchored member of the immunoglobulin superfamily related to chicken contactin. *J Cell Biol* 109(2):775–788.
10. Berglund EO, et al. (1999) Ataxia and abnormal cerebellar microorganization in mice with ablated contactin gene expression. *Neuron* 24(3):739–750.
11. Rios JC, et al. (2000) Contactin-associated protein (Caspr) and contactin form a complex that is targeted to the paranodal junctions during myelination. *J Neurosci* 20(22): 8354–8364.
12. Boyle ME, et al. (2001) Contactin orchestrates assembly of the septate-like junctions at the paranode in myelinated peripheral nerve. *Neuron* 30(2):385–397.
13. Faivre-Sarrailh C, et al. (2000) The glycosylphosphatidyl inositol-anchored adhesion molecule F3/contactin is required for surface transport of paranodin/contactin-associated protein (caspr). *J Cell Biol* 149(2):491–502.
14. Sherman DL, et al. (2005) Neurofascins are required to establish axonal domains for saltatory conduction. *Neuron* 48(5):737–742.
15. Salzer JL, Brophy PJ, Peles E (2008) Molecular domains of myelinated axons in the peripheral nervous system. *Glia* 56(14):1532–1540.
16. Kazarinova-Noyes K, et al. (2001) Contactin associates with Na+ channels and increases their functional expression. *J Neurosci* 21(19):7517–7525.
17. Koch T, Brugger T, Bach A, Gennarini G, Trotter J (1997) Expression of the immunoglobulin superfamily cell adhesion molecule F3 by oligodendrocyte-lineage cells. *Glia* 19(3):199–212.
18. White R, et al. (2008) Activation of oligodendroglial Fyn kinase enhances translation of mRNAs transported in hnRNP A2-dependent RNA granules. *J Cell Biol* 181(4):579–586.
19. Laursen LS, Chan CW, ffrench-Constant C (2009) An integrin-contactin complex regulates CNS myelination by differential Fyn phosphorylation. *J Neurosci* 29(29): 9174–9185.
20. Godement P, Salaün J, Imbert M (1984) Prenatal and postnatal development of retinogeniculate and retinocollicular projections in the mouse. *J Comp Neurol* 230(4): 552–575.
21. Huberman AD, et al. (2008) Architecture and activity-mediated refinement of axonal projections from a mosaic of genetically identified retinal ganglion cells. *Neuron* 59(3):425–438.
22. Shaw G, Weber K (1982) Differential expression of neurofilament triplet proteins in brain development. *Nature* 298(5871):277–279.
23. Brady ST, et al. (1999) Formation of compact myelin is required for maturation of the axonal cytoskeleton. *J Neurosci* 19(17):7278–7288.
24. Murtie JC, Macklin WB, Corfas G (2007) Morphometric analysis of oligodendrocytes in the adult mouse frontal cortex. *J Neurosci Res* 85(10):2080–2086.
25. Mallon BS, Shick HE, Kidd GJ, Macklin WB (2002) Proteolipid promoter activity distinguishes two populations of NG2-positive cells throughout neonatal cortical development. *J Neurosci* 22(3):876–885.
26. Wang H, Kunkel DD, Martin TM, Schwartzkroin PA, Tempel BL (1993) Heteromultimeric K+ channels in terminal and juxtaparanodal regions of neurons. *Nature* 365(6441):75–79.
27. Boiko T, et al. (2001) Compact myelin dictates the differential targeting of two sodium channel isoforms in the same axon. *Neuron* 30(1):91–104.
28. Kaplan MR, et al. (2001) Differential control of clustering of the sodium channels Na(v)1.2 and Na(v)1.6 at developing CNS nodes of Ranvier. *Neuron* 30(1):105–119.
29. Krämer-Albers E-M, White R (2011) From axon-glial signalling to myelination: The integrating role of oligodendroglial Fyn kinase. *Cell Mol Life Sci* 68(12):2003–2012.
30. Seiwa C, Sugiyama I, Yagi T, Iguchi T, Asou H (2000) Fyn tyrosine kinase participates in the compact myelin sheath formation in the central nervous system. *Neurosci Res* 37(1):21–31.
31. Perge JA, Koch K, Miller R, Sterling P, Balasubramanian V (2009) How the optic nerve allocates space, energy capacity, and information. *J Neurosci* 29(24):7917–7928.
32. Brümmendorf T, et al. (1993) The axonal recognition molecule F11 is a multifunctional protein: Specific domains mediate interactions with Ng-CAM and restrictin. *Neuron* 10(4):711–727.
33. Morales G, et al. (1993) Induction of axonal growth by heterophilic interactions between the cell surface recognition proteins F11 and Nr-CAM/Bravo. *Neuron* 11(6): 1113–1122.
34. Volkmer H, Zacharias U, Nörenberg U, Rathjen FG (1998) Dissection of complex molecular interactions of neurofascin with axonin-1, F11, and tenascin-R, which promote attachment and neurite formation of tectal cells. *J Cell Biol* 142(4):1083–1093.
35. Zeng L, D'Alessandri L, Kalousek MB, Vaughan L, Pallen CJ (1999) Protein tyrosine phosphatase α (PTPalpha) and contactin form a novel neuronal receptor complex linked to the intracellular tyrosine kinase fyn. *J Cell Biol* 147(4):707–714.
36. Barres BA, Raff MC (1999) Axonal control of oligodendrocyte development. *J Cell Biol* 147(6):1123–1128.
37. Wake H, Lee PR, Fields RD (2011) Control of local protein synthesis and initial events in myelination by action potentials. *Science* 333(6049):1647–1651.
38. Chatzopoulou E, et al. (2008) Structural requirement of TAG-1 for retinal ganglion cell axons and myelin in the mouse optic nerve. *J Neurosci* 28(30):7624–7636.
39. Yu T, Lieberman AP (2013) Npc1 acting in neurons and glia is essential for the formation and maintenance of CNS myelin. *PLoS Genet* 9(4):e1003462.
40. de Waegh SM, Lee VM, Brady ST (1992) Local modulation of neurofilament phosphorylation, axonal caliber, and slow axonal transport by myelinating Schwann cells. *Cell* 68(3):451–463.
41. Hsieh ST, et al. (1994) Regional modulation of neurofilament organization by myelination in normal axons. *J Neurosci* 14(11 Pt 1):6392–6401.
42. Sánchez I, Hassinger L, Paskevich PA, Shine HD, Nixon RA (1996) Oligodendroglia regulate the regional expansion of axon caliber and local accumulation of neurofilaments during development independently of myelin formation. *J Neurosci* 16(16): 5095–5105.
43. Câmara J, et al. (2009) Integrin-mediated axoglial interactions initiate myelination in the central nervous system. *J Cell Biol* 185(4):699–712.
44. Dupree JL, Girault J-A, Popko B (1999) Axo-glial interactions regulate the localization of axonal paranodal proteins. *J Cell Biol* 147(6):1145–1152.
45. Bhat MA, et al. (2001) Axon-glia interactions and the domain organization of myelinated axons requires neurexin IV/Caspr/Paranodin. *Neuron* 30(2):369–383.
46. Rios JC, et al. (2003) Paranodal interactions regulate expression of sodium channel subtypes and provide a diffusion barrier for the node of Ranvier. *J Neurosci* 23(18): 7001–7011.
47. Dupree JL, Coetzee T, Blight A, Suzuki K, Popko B (1998) Myelin galactolipids are essential for proper node of Ranvier formation in the CNS. *J Neurosci* 18(5): 1642–1649.
48. Susuki K, et al. (2013) Three mechanisms assemble central nervous system nodes of Ranvier. *Neuron* 78(3):469–482.
49. Rasband MN, et al. (1999) Dependence of nodal sodium channel clustering on paranodal axoglial contact in the developing CNS. *J Neurosci* 19(17):7516–7528.
50. Rosenbluth J, Dupree JL, Popko B (2003) Nodal sodium channel domain integrity depends on the conformation of the paranodal junction, not on the presence of transverse bands. *Glia* 41(3):318–325.
51. Peles E, et al. (1995) The carbonic anhydrase domain of receptor tyrosine phosphatase β is a functional ligand for the axonal cell recognition molecule contactin. *Cell* 82(2): 251–260.
52. Nörenberg U, Hubert M, Brümmendorf T, Tárnok A, Rathjen FG (1995) Characterization of functional domains of the tenascin-R (restrictin) polypeptide: cell attachment site, binding with F11, and enhancement of F11-mediated neurite outgrowth by tenascin-R. *J Cell Biol* 130(2):473–484.
53. Rigato F, et al. (2002) Tenascin-C promotes neurite outgrowth of embryonic hippocampal neurons through the alternatively spliced fibronectin type III BD domains via activation of the cell adhesion molecule F3/contactin. *J Neurosci* 22(15):6596–6609.
54. Rush AM, et al. (2005) Contactin regulates the current density and axonal expression of tetrodotoxin-resistant but not tetrodotoxin-sensitive sodium channels in DRG neurons. *Eur J Neurosci* 22(1):39–49.
55. Brackenbury WJ, et al. (2008) Voltage-gated Na+ channel beta1 subunit-mediated neurite outgrowth requires Fyn kinase and contributes to postnatal CNS development in vivo. *J Neurosci* 28(12):3246–3256.
56. Barres BA, Raff MC (1993) Proliferation of oligodendrocyte precursor cells depends on electrical activity in axons. *Nature* 361(6409):258–260.
57. Demerens C, et al. (1996) Induction of myelination in the central nervous system by electrical activity. *Proc Natl Acad Sci USA* 93(18):9887–9892.
58. Malone M, et al. (2013) Neuronal activity promotes myelination via a cAMP pathway. *Glia* 61(6):843–854.
59. Stevens B, Porta S, Haak LL, Gallo V, Fields RD (2002) Adenosine: A neuron-glial transmitter promoting myelination in the CNS in response to action potentials. *Neuron* 36(5):855–868.
60. Kazarinova-Noyes K, Shrager P (2002) Molecular constituents of the node of Ranvier. *Mol Neurobiol* 26(2-3):167–182.
61. Rothe C, et al. (2008) The human combinatorial antibody library HuCAL GOLD combines diversification of all six CDRs according to the natural immune system with a novel display method for efficient selection of high-affinity antibodies. *J Mol Biol* 376(4):1182–1200.
62. Gallyas F (1979) Silver staining of myelin by means of physical development. *Neurol Res* 1(2):203–209.
63. Friedrich VL, Mugnaini E (1981) Preparation of neural tissues for electron microscopy. *Neuroanatomical Tract-Tracing Methods*, eds Heimer L, Robards MJ (Plenum, New York), pp 345–375.